View Article Online
DOI: 10.1039/C8LC01416G

AC electrokinetic biased Deterministic Lateral Displacement for tunable particle separation

Victor Calero [a], Pablo Garcia-Sanchez [b], Carlos Honrado [a], Antonio Ramos [b] and Hywel Morgan [a]

[a] School of Electronics and Computer Science, and Institute for Life Sciences, University of Southampton, United Kingdom.

[b] Departamento de Electrónica y Electromagnetismo, Facultad de Física, Universidad de Sevilla, Spain.

Abstract

We describe a novel particle separation technique that combines deterministic lateral displacement (DLD) with orthogonal electrokinetic forces. DLD is a microfluidic technique for continuous flow particle separation based on size. We describe new tunable devices that use a combination of AC electric fields with DLD to separate particles below the critical diameter. Planar electrodes were integrated into a classical DLD device to produce a force orthogonal to the fluid flow direction. Experiments with 3.0 µm, 1.0 µm and 500 nm diameter microspheres show that at low frequencies (up to 500 Hz) particles oscillate in the direction of the field due to Electrophoretic (EP)/Electroosmotic (EO) forces. As the frequency of the field increases, the amplitude of these oscillations vanishes and, eventually dielectrophoresis (DEP) becomes the dominant electrokinetic force on the particles (DEP arises from electric field inhomogeneities caused by the presence of the DLD posts). Both mechanisms alter the paths of the particles inside the DLD devices leading to enhanced sorting of particles below the critical diameter of the device.

Introduction

Almost every biological sample is composed of mixtures of cells, vesicles and macromolecules of different types and properties and the separation and purification of sub-sets of micrometre and sub-micrometre particles is an essential step in many analytical processes. However, current separation techniques are time consuming and often require large amounts of sample. To address this, a range of different microfluidic separation technologies has been developed. One of the most promising is Deterministic Lateral Displacement (DLD) which is a passive particle separation technique that uses an array of circular posts to separate particles based on size; particles larger than a critical diameter (D_c) are separated from smaller particles in a continuous flow. The method was first reported by Huang *et al* in 2004 [1] and has been extensively studied since then [2–4]. Many research groups have explored this technique and have modified the geometry of the devices to improve efficiency and extend the range of potential applications. *Loutherback et al* [5] demonstrated successful separation of particles using triangular posts rather than cylinders to reduce the critical diameter with respect to the gap between the posts, resulting in a reduced risk of clogging and a lower hydrostatic pressure. *Liu et al* [6] used similar triangular posts for isolation of Circulating Tumor Cells (CTCs) from spiked blood samples demonstrating enhanced efficiency. Non-cylindrical posts also improve the separation of non-spherical particles and *Zeming et al* [7] showed how I-shaped posts could be used to separate non-spherical particles like Red Blood Cells (RBCs). Asymmetrical DLD devices have also been made [8], where different lateral and horizontal gaps led to improved separation efficiency and throughput over traditional symmetric DLD arrays where enhanced sorting of non-spherical particles was shown. In [9] a staggered DLD was used for fractionation of sub-micrometre particles of several using a device with different sections of increasing critical diameters fabricated within the same channel, each section responsible for separating particles of a specific size.

DLD devices have been successfully used to separate biological and non-biological particles based not only on size but also on other properties like shape [7] or deformability [10]. Recently it was shown that the principle could be scaled to enable the separation of very small particles in the range of nanometres like exosomes [11]. Further modifications include the addition of external forces to the system to increase the range of separation possibilities. For example *Devendra et al* [12] used a gravitational force to both drive the fluid and the particles through the devices and tune the separation. *Beech et al* [13] developed a tunable DLD by applying strain to an elastomeric DLD device to modify the dimensions of the array of posts. The same group were the first to demonstrate the combination of AC electrokinetic forces (dielectrophoresis) with DLD [14]. They placed an electrode at the inlet and the outlet of a mirrored DLD device creating an electric field along the channel, in the direction of the fluid flow. They reported tunable separation of 5 µm and 3 µm diameter polystyrene beads in a 6.0 µm critical diameter DLD using a 100 Hz AC electric field. The induced deviation of particles smaller than the critical diameter was attributed to the action of DEP forces on the flowing particles due to the non-uniform electric field created by the presence of the insulating posts. *Zeming et al* [9] recently reported that electrostatic forces between pillars and nano-scale particles can be modulated by the electrolyte salt concentration that modifies the apparent particle and post size by changing the double layer repulsion, with measurable effects on the performance of micron-sized DLD for separation of nanoparticles.

View Article Online
DOI: 10.1039/C8LC01416G

A commonly used separation technique termed insulator-based Dielectrophoresis (iDEP) has been used by several groups [15]. It consists of an array of insulating structures fabricated in a channel to create a spatial electric field gradient. Conventional DEP techniques utilise patterned metal electrodes with different geometries to create the required electric field gradients [16], but this is only in 2D. By contrast, iDEP can produce 3D field gradients using structures of insulating materials, such as plastic or polymers. These are in general easier to make and simplify the fabrication procedures, enabling mass-fabrication, and have convenient properties like flexibility or transparency [17].

The general principle of iDEP was first reported by Masuda *et al* [18] in 1989. They utilised a constriction between two electrodes to trap cells by DEP and induce fusion. Since then many researchers have reported devices with different geometries covering a wide range of applications for microparticle manipulation and separation. *Cummings et al.* [19–21] used arrays of insulating posts, to generate non-uniform electric fields within a channel demonstrating DEP focusing and trapping of particles. Similar devices have been used by Lapizco-Encinas and co-workers for enrichment and trapping of different particles, like bacteria and proteins [22–24]. Although iDEP devices have shown great potential for particle trapping and enrichment, these devices based on arrays of insulating posts lack the ability to separate particles in a continuous flow.

Other iDEP devices with different geometries have been developed for this purpose. For example, *Srivasta et al* [25] described particle separation using DC-iDEP with insulating rectangular obstacles placed in the channel, while the fluid was also pumped by the electric field. Similarly, *Lewpiriyawong et al* [26] utilised a microfluidic H-filter with several constrictions within the channel to produce a DEP force and control separation of micron-sized particles. Different geometries have also been reported for continuous flow separation by iDEP [27–30]

In this article, a new tunable DLD technique is described that applies an AC field of variable frequency orthogonal to the particle flow direction. Two coplanar electrodes are placed either side of a single DLD channel generating electrokinetic forces to control particle behaviour. High electric field gradient zones are generated in the vicinity of the insulating posts inducing deviation of particles smaller than the critical diameter. Particles are affected either by DEP (similar to [14]) at all frequencies > 100 Hz, or oscillating electrophoretic and electroosmotic forces at low frequencies. This electrode configuration has an electrode spacing of a few mm, much less than previous publications where the electrodes are placed at the inlet and oulet of the DLD/iDEP channels. Consequently, much smaller voltages are required to generate similar electric fields. This electrode configuration also means that a much wider frequency range (up to MHz) can be used. This compares with conventional devices where electrode spacing is of the order of a few centimetres requiring thousands of volts with limited frequency range.

Combining the versatility of electrokinetics with the precision of DLD enables separation of particles in a continuous flow. Unlike continuous flow iDEP separation techniques, the forces are not applied at specific points in the channel; separation occurs gradually as particles flow through the array, similar to traditional DLD. In this paper the behaviour of the system is analysed as a function of the applied AC frequency and suspending electrolyte conductivity along with a preliminary analysis of the experimental observations.

DLD theory

The principles of DLD have been extensively described [4,31]. This passive technique exploits the broken symmetry of an array of offset pillars within a conventional laminar flow. The simplest DLD devices consist of an array of circular posts placed at a given centre-to-centre distance λ within the same column. The gap G between posts is equal to the post diameter D_p, so that $\lambda = D_p + G$. The next column is at the same spacing λ but shifted a certain lateral distance $\Delta\lambda$ from the previous column (see Figure 1a). The periodicity N of this geometry in the downstream direction is given by:

$$N = \frac{\lambda}{\Delta\lambda} \quad (1)$$

The tilt angle θ of the rows of posts is related to the period of the array N:

$$\tan(\theta) = \frac{\Delta\lambda}{\lambda} = \frac{1}{N} \quad (2)$$

This geometry defines a critical particle diameter D_c, where particles bigger than D_c are separated from the smaller particles. The principle of operation of DLD is described schematically in Figure 1b. As show, in the figure, a stagnation point is found either side of each pillar. On the upstream side of one pillar (left side of the posts in Figure 1b); streamlines that end at stagnation points separate the fluid that passes above the post from the fluid that passes below (see example posts A and B in Fig 1b). Following Kim *et al* [31], we adopt the term separatrix to define a streamline that starts at a stagnation point on a pillar and ends on a pillar that is exactly N rows downstream as shown in Fig 1b.

View Article Online
DOI: 10.1039/C8LC01416G

The critical diameter of the device D_c, corresponds to twice the minimum distance between post A and the separatrix that ends in post B. Particles bigger than D_c are forced to cross the separatrix as they interact with the posts, passing above the next post so that the particles start bumping; this behaviour is termed displacement mode. Particles smaller than D_c do not cross the separatrix, but pass below the post, and keep flowing following the fluid, zigzagging around the posts, in the so-called zig-zag mode. This process is repeated every time a particle interacts with the post and is magnified as the particles flow along the channel. After many successive bumps the particles separate into two populations with diameters bigger and smaller than D_c, as shown in Figure 1b. The deviation angle is defined as the tilt angle of the rows of posts, θ.

Davis derived an empirical formula to estimate D_c from the geometrical parameters of the array, assuming spherical particles in an array of circular posts [32]:

$$D_c = 1.4GN^{-0.48} \quad (3)$$

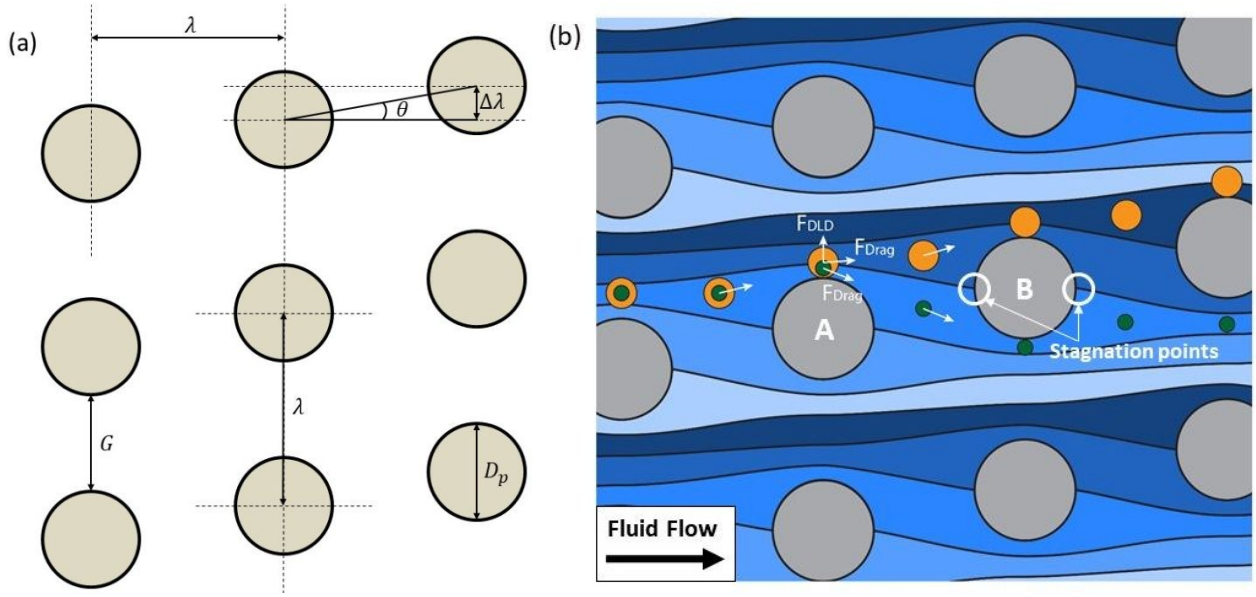

Figure 1 Schematic diagram of a DLD array. (a) Parameters that define the geometry of the array of circular posts in a DLD channel. (b) Paths followed by particles in a DLD device together with forces on the particles. Stagnation points are located at both sides of the posts, where the separatrices (black lines) start and end. Particles bigger than D_c (orange) are forced to cross the separatrix when interacting with the posts, entering the bumping mode whereas particles smaller (green) than the D_c flow in a zigzag manner around the posts.

Electrokinetic forces: Electrophoresis, Electroosmosis and Dielectrophoresis

- **Electrophoresis (EP) and Electroosmosis (EO)**

When a charged surface is immersed in an electrolyte, the ions in suspension effectively screen the surface charge and electroneutrality is maintained. When an electric field is applied, a force is exerted on the cloud of ions of opposite charge to the surface. This force gives rise to relative motion between the liquid and solid. The fluid flow relative to a stationary surface is termed Electroosmosis (EO). The ratio between the fluid velocity v and the magnitude of the electric field E is the electroosmotic mobility μ_{EO}, defined by the Helmholtz-Smoluchowsky equation:

$$\mu_{EO} = \frac{v}{E} = -\frac{\varepsilon_m \zeta_s}{\eta} \quad (4)$$

where ε_m is the permittivity of the medium, η the dynamic viscosity and ζ_s is the zeta potential of the surface, the electrical potential at the slip plane [33–36].

Likewise, when a charged particle is immersed in a quiescent liquid, the relative motion between the liquid and solid results in particle motion. This movement is called electrophoresis (EP) and the ratio between the particle velocity v and the magnitude of the electric field E is the electrophoretic mobility μ_{EP}, defined by the same equation, the Helmholtz-Smoluchowski equation:

$$\mu_{EP} = \frac{v}{E} = \frac{\varepsilon_m \zeta_p}{\eta} \quad (5)$$

View Article Online
DOI: 10.1039/C8LC01416G

where ζ_p is the zeta potential of the particle. In the case of a particle within a microchannel, both forces act on the particle and the total electrokinetic mobility is the sum of both, the electrophoretic and electroosmotic mobilities:

$$\mu_{EK} = \mu_{EO} + \mu_{EP} \quad (6)$$

- **Dielectrophoresis (DEP)**

Dielectrophoresis is the force exerted by a non-uniform electric field on a polarisable particle suspended in an electrolyte [33,37,38]. If the polarisabilities of medium and particle are different, the application of an electric field leads to the creation of an induced dipole across the particle. The magnitude and direction depend on both the properties of the medium and the particle. If the electric field is spatially uniform, the force exerted on each pole is the same and the net force is zero. However, if the electric field is spatially non-uniform the force acting on each pole is different leading to movement called DEP. For a spherical dielectric particle the DEP force is given by [33]:

$$\langle \vec{F}_{DEP} \rangle = 2\pi\varepsilon_m a^3 Re[\tilde{f}_{CM}] \nabla |\vec{E}|^2 \quad (7)$$

where a is the particle radius and $\tilde{f}_{CM}$the Clausius-Mossotti factor:

$$\tilde{f}_{CM} = \frac{\tilde{\varepsilon}_p - \tilde{\varepsilon}_m}{\tilde{\varepsilon}_p + 2\tilde{\varepsilon}_m} \quad (8)$$

The indices p and m refer to the particle and medium respectively, and $\tilde{\varepsilon}_p$ and $\tilde{\varepsilon}_m$ are the complex permittivities, defined as $\tilde{\varepsilon} = \varepsilon - i\sigma/\omega$, where σ is the conductivity and ω the frequency of the field. The magnitude of the DEP force depends on the gradient of the electric field and has two different directions depending on the sign of the real part of $\tilde{f}_{CM}$. If the particle is less polarisable than the medium, $\mathrm{Re}[\tilde{f}_{CM}] < 0$ and the particle is repelled from regions of high electric field gradient; this is called negative DEP (nDEP). Conversely, if the particle is more polarisable than the medium, $\mathrm{Re}[\tilde{f}_{CM}] > 0$ and it is attracted to the high electric field regions; termed positive DEP (pDEP). The particle polarisation depends on the frequency of the electric field meaning that the DEP direction can be controlled by changing the frequency. It also depends on the complex permittivity of the suspending electrolyte, so that changing the conductivity of the electrolyte also controls the DEP properties.

For solid insulating particles the particle conductivity dominates the behaviour at low frequencies. The total particle conductivity is given by the sum of the bulk conductivity $\sigma_{p,b}$ and the surface term $\sigma_{p,s}$ given by:

$$\sigma_{p,s} = \frac{2K_s}{a} \quad (9)$$

where K_s is the surface conductance [39,40], which is typically around 1nS. Thus, for large diameter particles (>1 μm) their DEP behaviour is always negative across all frequencies (except for extremely low conductivity electrolytes). However, nano-particles can have a conductivity greater than the suspending electrolyte leading to pDEP. This is illustrated in Figure 2 where the frequency dependence of the Clausius-Mossotti factor for different particle sizes and electrolyte conductivity is plotted. At high frequencies (>1MHz) particle behaviour is dominated by particle permittivity which is always lower than the suspending electrolyte and, therefore, all solid particles eventually experience nDEP for frequencies larger than 1MHz. Figure 2 depicts the results of the Maxwell-Wagner-O'Konski relaxation mechanism [36]. Note that the so-called alpha-relaxation has not been considered [41]. This relaxation mechanism appears for frequencies of the order of $f_\alpha = D/(2\pi a^2)$, where *D* is the diffusion constant of the ions. For the particles used in this work ($2a = 1, 3$ μm), the alpha-relaxation appears for frequencies around $10 - 100$ Hz. For positive particle polarisabilities, it is expected that this leads to a small decrement in the induced dipole amplitude for $f < f_\alpha$, but the effect is negligible for negative polarisabilities.

View Article Online
DOI: 10.1039/C8LC01416G

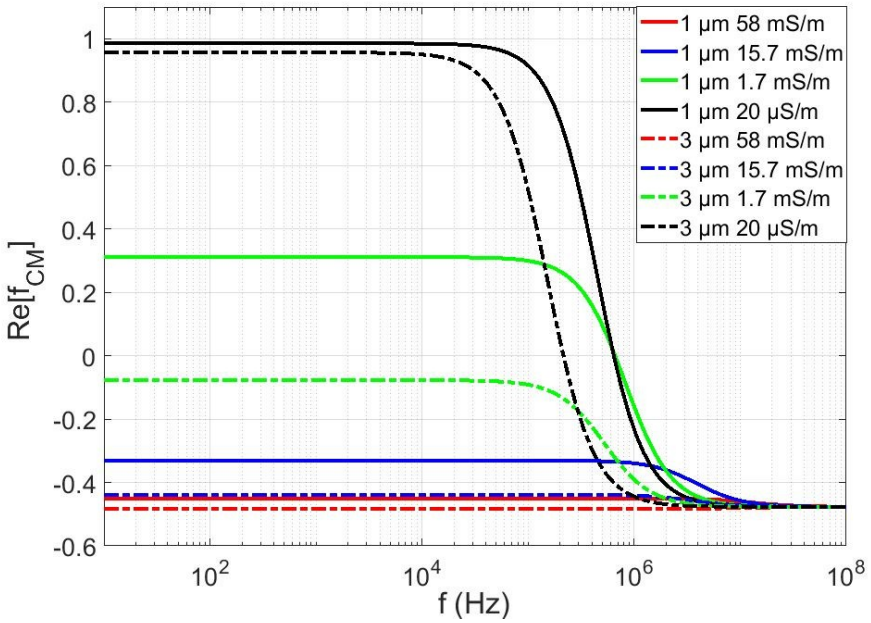

Figure 2. Change in $Re[\tilde{f}_{CM}]$ *for a solid dielectric sphere as a function of the frequency of an AC electric field for different particle sizes and electrolyte conductivities* ($\varepsilon_m = 80\varepsilon_0, \varepsilon_p = 2.5\varepsilon_0, \sigma_p \approx \sigma_{p,s}, K_s = 1\ nS$).

Electrokinetically biased DLD

Figure 3a shows a 2-D plot of the field gradient together with the fluid streamlines for an electric field applied along the direction of the fluid flow (as in ref. [14]), while Figure 3b shows the field gradient for an electric field applied perpendicular to the fluid flow. When the electric field is parallel to the flow, the high electric field regions are in between the posts along the direction of the streamlines. In ref. [14] it was shown that high electric field gradients push particles to cross the separatrix by nDEP when they pass close to the posts. As depicted in Figure 3a, even if a particle is smaller than the critical diameter, the nDEP force generated by the field gradient around the insulating pillar has the same effect as a hydrodynamic interaction with a post, displacing the particle that enters the displacement mode. A similar behaviour is observed when the electrodes generate a field orthogonal to the flow (Figure 3b).

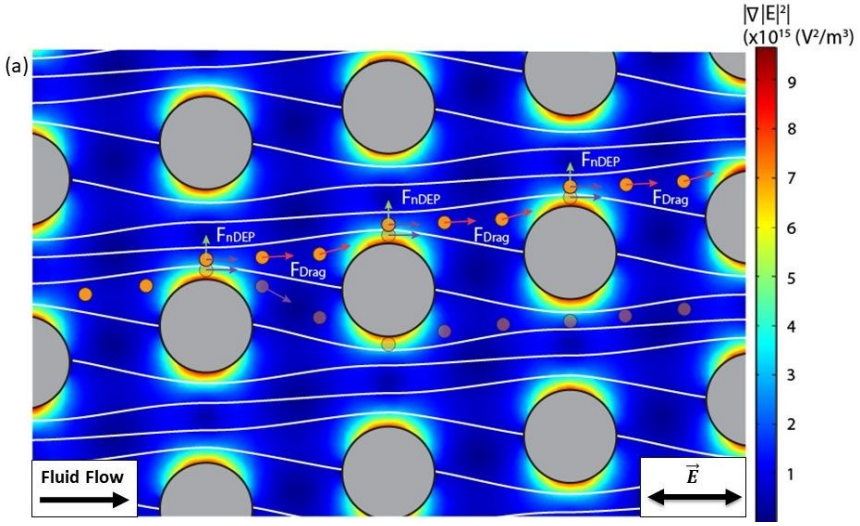

View Article Online
DOI: 10.1039/C8LC01416G

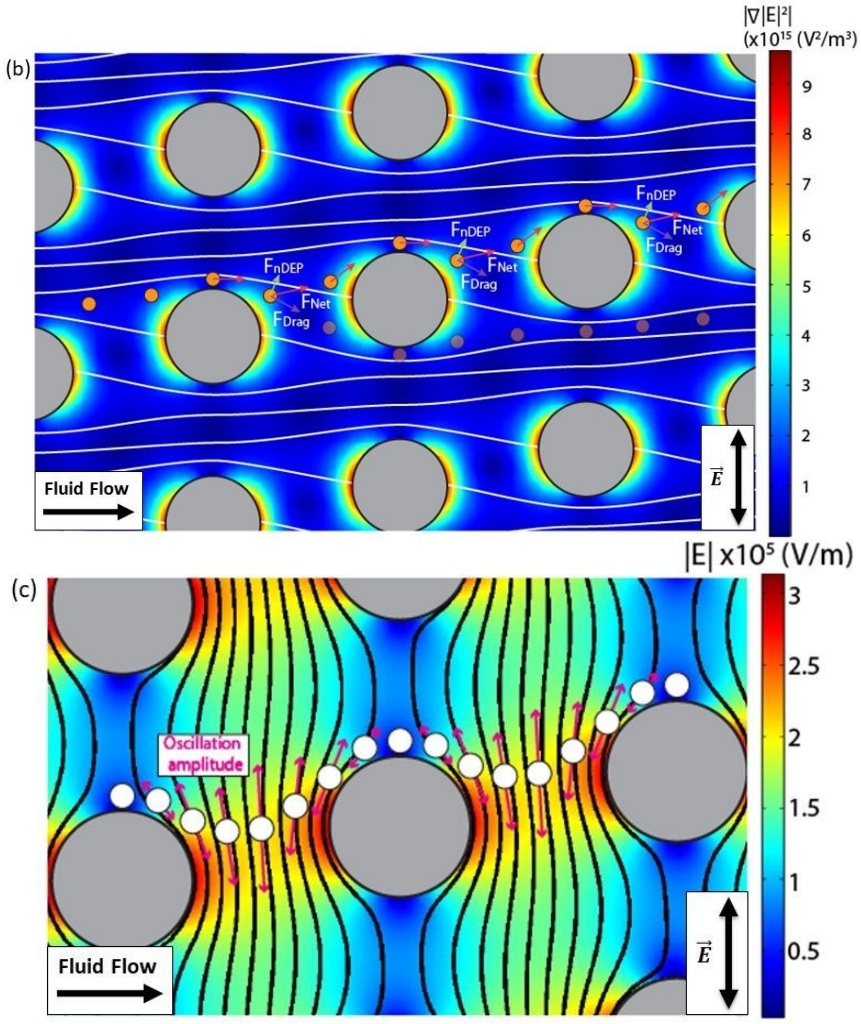

Figure 3. Schematic diagrams summarising the electrokinetic behaviour of particles inside a DLD. The particle trajectories represented do not correspond with calculated trajectories and are only a qualitative representation of the behaviour that agree with experimental observations. (a) nDEP induced deviation of a particle, as reported in [14]; the nDEP force pushes the particle to cross the separatrix when it passes close to a post. (b) nDEP induced deviation with the field orthogonal to the flow; the nDEP force prevents particles from zigzagging when trying to pass between the posts of the same row. (c) Diagram of the low frequency induced deviation of a particle. The oscillation of the particles along the field lines and perpendicular to the fluid flow due to electrophoresis and electroosmosis changes the effective diameter of the particle, leading to deviation.

In the configuration presented in this work, the high electric field gradients are located between posts of the same row (Fig 3(b)). In order for particles smaller than the critical diameter to flow without deviation, they must follow the fluid flow direction, zigzagging between the posts. However, if these particles experience nDEP, the force acts mainly orthogonally to the Stokes force created by the fluid flow. If the nDEP force is strong enough, particles are prevented from zigzagging and start bumping along the posts, flowing in displacement mode (see Fig 3b). At low frequencies (below 1 kHz), particles are observed to enter a different mode of behaviour where the force is controlled by the superposition of DLD and an oscillating DC, electrophoretic and electroosmotic force which creates a low frequency oscillation of the particle along the direction of the electric field lines. This oscillation is superimposed on a non-zero DEP force (in the low frequency range), and modifies the effective particle diameter, leading to deviation of particles smaller than the critical diameter as illustrated schematically in Fig. 3c. Both these mechanisms (nDEP at high frequency and EP/EO at low frequency) change the dynamics of the DLD separation system so that the deviation of particles through the device can be tuned using an external electric field.

As mentioned above, the application of an orthogonal field enables lower voltages to be used, and thus a wider frequency range. In addition, it enables the study of low frequency electrokinetic forces in a direction perpendicular to the fluid flow within DLD devices. In ref. [14] the electrokinetically induced particle deviation was solely attributed to DEP, even though low frequency (100 Hz) electric fields were used. In this work we show that both EP and EO are significant at these frequencies and could have played a role in the mechanism reported in [14].

View Article Online
DOI: 10.1039/C8LC01416G

Materials and methods

Electric field and fluid flow simulations

To calculate the electric field distribution and the fluid velocity field around the posts, a 2-D finite element simulation was performed using the commercial software COMSOL Multiphysics® v.5.3 (COMSOL AB, Stockholm, Sweden). The results are presented in Figure 3. For the electric field calculation the Laplace equation was solved in the liquid with the pillars considered to be perfect insulators. For the hydrodynamic problem, the Stokes equation was solved with no slip boundary conditions on the posts walls. The simulation domain consisted of a large DLD array of posts and the images for Figure 3 were taken from a solution in the central region of the domain.

DLD device

The DLD device used in this work uses a sheath flow to confine the particle stream, as shown in Figure 4. It has three inlets; the central inlet (towards the bottom of the device) is used to introduce the sample. The other two inlets control the sheath flow and focus the sample stream from inlet to outlet. In the absence of any deflection, the deviation angle of particles flowing through the device is by definition zero degrees and the particle exit from the bottom outlet. However, any force will deflect particles away from the central axis, and experimentally this is measured by comparing the position where the particles enter the channel to the total lateral displacement at the end of the array. The sheath flow also prevents the majority of electrolysis products produced at the electrodes from interfering with the sample stream and prevents particles from trapping at the electrodes. At the end of the channel there are two outlets, one to collect the deviated particles and another to collect particles flowing in zig-zag mode. Particles that are deflected in the bump or displacement mode accumulate in the upper part of the device and exit from the upper of the two outlets. The DLD device consists of a simple array of offset circular posts with a diameter D_p of $18\ \mu m$. The array is symmetric with gap between the posts equal to the post diameter ($G = D_p$). This geometry defines a critical diameter of $6.3\ \mu m$ (according to eq. 3) and a maximum deviation angle of 3.18^{o}. The dimensions of the channel were $2.6\ mm \times 31.7\ mm$ with an average channel depth of $8\ \mu m$. A diagram of the DLD design is shown in Figure 4.

Samples

The particles used were fluorescent carboxylate polystyrene microspheres of 0.5 μm, 1.0 μm and 3.0 μm diameter with coefficients of variation of 3%, 3% and 5 % respectively (Fluoresbrite® YG Carboxylate Microspheres). They were suspended in KCl with conductivities of 1.7 mS/m, 6.6 mS/m, 15.7 mS/m and 58 mS/m.

Experimental

The DLD devices were made from PDMS (Polydimethylsyloxane), cast from a silicon master fabricated using standard photolithography, and bonded using plasma-activated bonding to a glass substrate with patterned platinum electrodes. The electrodes consisted of two parallel plates $31.3\ mm$ long, separated by a $2.2\ mm$ gap. The electrodes were connected to a signal generator (TTi, Inc TGA12104) and a 50x amplifier (Falco Systems High Voltage Amplifier WMA-300) that delivered up to 320 Vpp at frequencies up to 1 MHz. This produced an AC electric field with a maximum magnitude of 150 kV/m. To filter out any residual DC offset a 10 μF capacitor was connected in series with the amplifier. Fluid flow was controlled independently at each of the three inlets – the sheath flow inlets and the sample inlet – with a pressure controller with 3 channels, (Elveflow® OB1 MK3) that delivers an accurate flow rate using a pressure-driven pump.

View Article Online
DOI: 10.1039/C8LC01416G

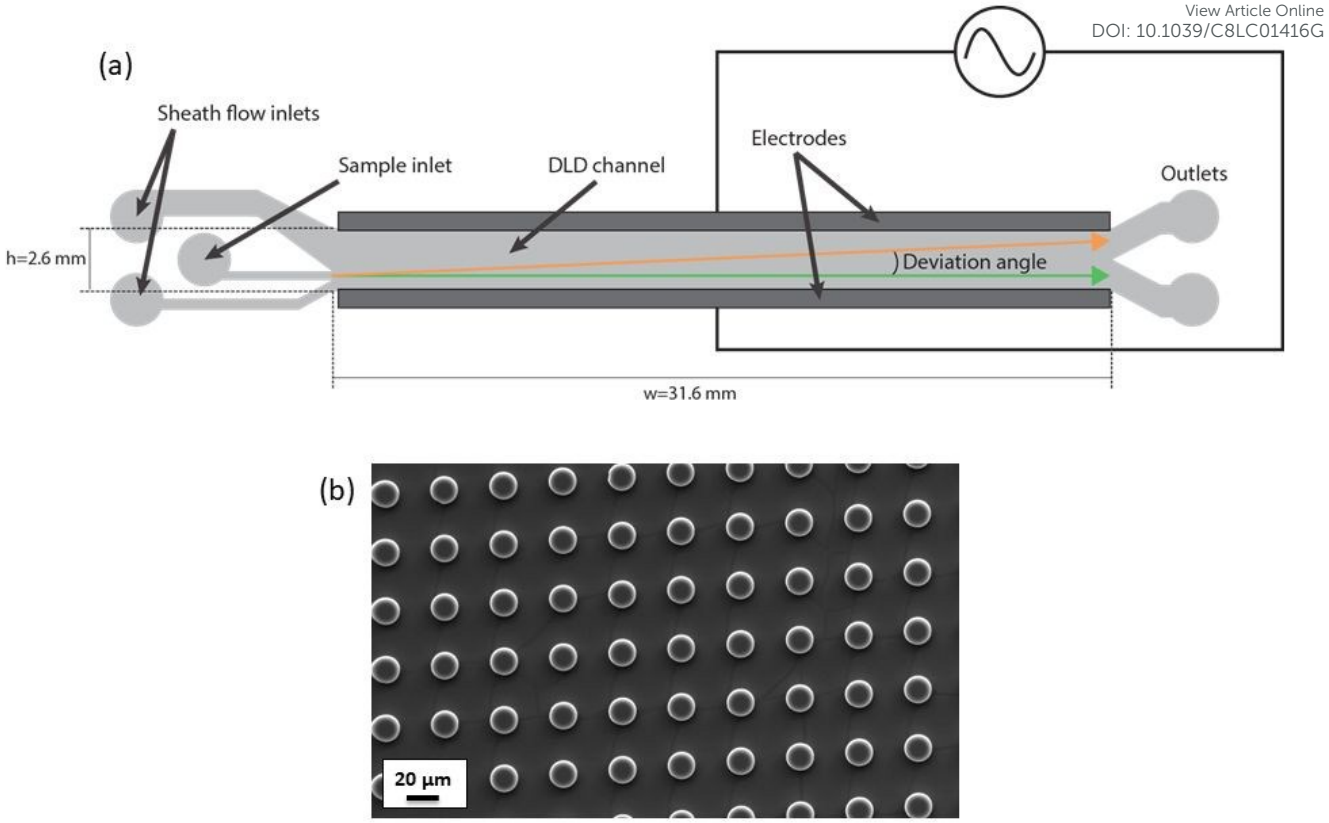

Figure 4 (a) Diagram of the experimental setup. Two planar platinum electrodes are placed alongside the channel creating an electric field perpendicular to the fluid flow. The sample is introduced via the central inlet and the pressure is controlled in the three inlets to ensure particles flow horizontally in a single stream with the same width as the sample inlet. (b) SEM picture of the posts in the DLD array.

Results and discussion

DLD without fluid flow

To understand the effects of the AC electric fields on particle behaviour, experiments were first done in the absence of any fluid flow. This enabled analysis of the electrokinetic behaviour of the particles to confirm that their behaviour matched theory. Images of particle movement for different frequency regimes are shown in Fig 5. Significant differences in behaviour were observed between low frequency (50 Hz - 500 Hz) and high frequency (above 500 Hz) signals. There was a predictable difference between the nDEP and the pDEP behaviours, which depended on the electrolyte conductivity.

Similar to iDEP devices, the array of insulating PDMS posts within the channel perturbs the electric field and creates zones of high and low electric field gradient between posts as shown in Figure 3. These regions of field gradient give rise to a DEP force that acts on particles as they flow through the channel. In general, when AC electric fields are used in iDEP systems the effects of electrophoresis and electroosmosis are ignored since for high frequencies the direction of the force changes too fast to produce an observable effect. However, at low enough frequencies (below 500 Hz), particles have sufficient time to move before the electric field changes direction and the time averaged electrophoretic effects can be non-zero. At low frequencies, particles oscillate along the direction of the electric field lines with the same frequency as the applied AC electric field. We observed that this low-frequency oscillation plays a significant role in the behaviour of particles within the DLD device.

For high frequencies (above 500 Hz), the particle behaviour is governed solely by DEP forces. When the particles are more polarisable than the medium ($\mathrm{Re}[\tilde{f}_{CM}] > 0$), they are attracted to the high electric field gradient regions between the posts (see Figure 5a). Conversely, when particles are less polarisable than the medium ($\mathrm{Re}[\tilde{f}_{CM}] < 0$), they are repelled from the high electric field gradient regions between the posts and concentrate in the low electric field gradient regions (see Figure 5b). In these conditions the DLD array behaves much as a normal iDEP trapping device.

View Article Online
DOI: 10.1039/C8LC01416G

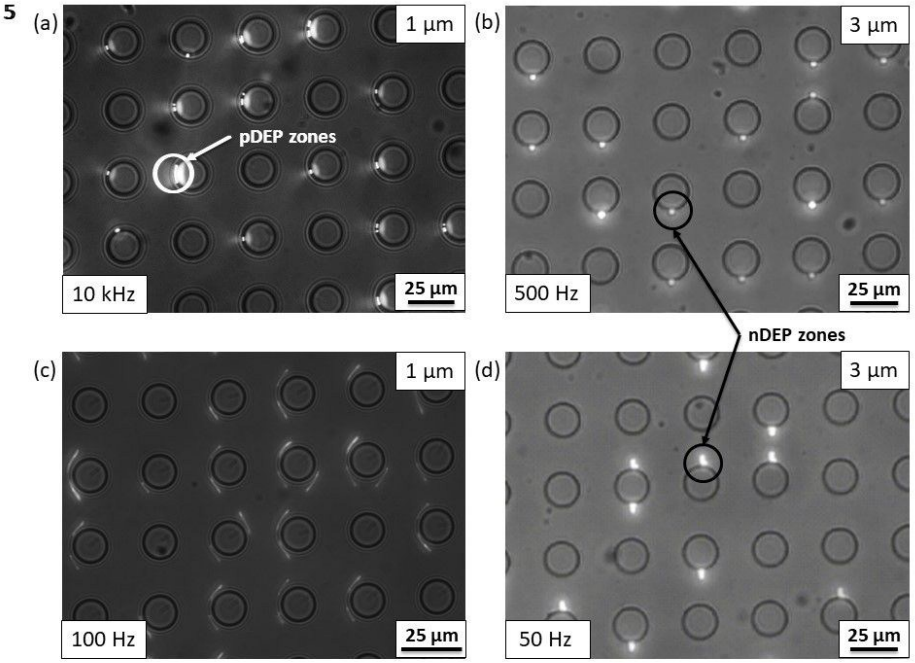

Figure 5 Electrokinetic behaviour in the DLD devices in the absence of fluid flow for an applied voltage of 320 Vpp. (a) pDEP trapping of 1.0 µm microspheres in DI water in the high electric field gradient regions for an applied signal of 10 kHz. (b) nDEP trapping of 3.0 µm microspheres in a 15.7 mS/m KCl solution for an applied signal of 500 Hz. (c) Oscillation of 1.0 µm microspheres at intermediate positions between the high and low electric field regions caused by applied signal of 100 Hz in DI water. (d) nDEP trapping of 3.0 µm microspheres in a 15.7 mS/m KCl solution for an applied signal of 50 Hz, the oscillation reduced drastically when the particles reached the minimum field position.

For low frequency AC electric fields (below 500 Hz), it was observed that the particles oscillate along the direction of the electric field lines due to a combination of EP and EO, which dominates at these frequencies. The oscillation is synchronous with the electric field, but because the posts distort the magnitude of the electric field, the amplitude of particle oscillation depends on the position of the particles with respect to the posts, as shown in Fig. 3c.

Although EP and EO dominate at low frequencies, a non-zero DEP force is still present. Particles that experience nDEP were pushed away from the zones of high electric field gradient whilst continuing to oscillate due to low frequency electrophoretic and electroosmotic forces. These particles move to an equilibrium position where the magnitude of the field is minimum, and the induced oscillation reduces drastically as shown in Figure 5d (see also Figure 3c). The equilibrium position in this case was similar to that observed at higher frequencies, where electrokinetic-induced oscillation is negligible. For particles more polarisable than the medium, the combination of pDEP with the low frequency oscillation moves particles to an equilibrium position with at an intermediate position between the high and low electric field regions, but almost in contact with the posts as shown in Figure 5c. The pDEP forces attract particles towards the high gradient electric field regions around the posts, where both the field gradient and the amplitude of the low frequency oscillation are maximum, this situation is unstable, and particles ultimately oscillate around the equilibrium positions shown in Figure 5c.

DLD with hydrodynamic flow

In the presence of an external fluid flow, the same electrokinetic forces are present but particles now experience a Stokes force. The trajectories of the particles through the DLD array are therefore modulated by a combination of EP/EO and DEP forces, and the action of these forces mean that particles smaller than the critical diameter can be fully deflected.

In the absence of any additional perturbation, particles smaller than the critical diameter move in zig-zag mode through the device; they pass between posts of the same row, not crossing the separatrices (see Figure 6a). However, when an AC electric field is applied perpendicular to the flow direction, the high electric field gradient regions created between the posts generates a DEP force. For particles that experience nDEP, the force acts mainly orthogonal to the Stokes force of the fluid and if the force is strong enough, particles are prevented from zigzagging through the device, changing their behaviour so that they bump between the posts, i.e. they transition into displacement mode. This is shown in Figure 6b.

When particles experience pDEP, their behaviour was not significantly affected, and they remained in zig-zag mode (if they were smaller than the critical diameter). Increasing the voltage applied to the electrodes eventually led to trapping of particles in the high electric field gradient regions by pDEP, but no displacement mode was observed.

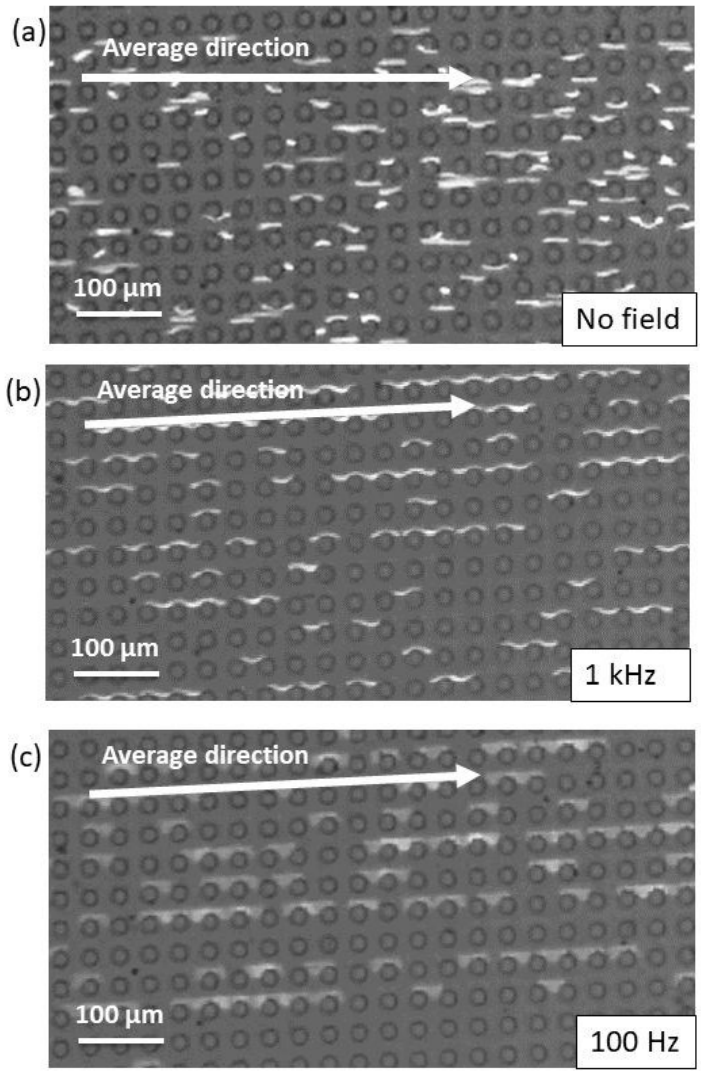

Figure 6 Electrokinetically induced deviation of 3.0 µm microspheres in a $D_c = 6.3$ µm DLD device for an electrolyte conductivity of 15.7 mS/m. (a) Particles zig-zag in the absence of an electric field. (b) nDEP induced displacement for a 1 kHz, 320 Vpp voltage signal. (c) Low frequency oscillation induced displacement for a 100 Hz, 320 Vpp voltage signal.

These observations are similar to the results reported in [14] where the field was applied along the direction of flow and the particle deviation attributed to nDEP. However, when the field is parallel to the flow direction the high electric field gradient regions are in a different place on the pillars (rotated by 90º - see Fig 3) and particle behaviour is different. Instead of particles being pushed away from the post when they pass close to the posts, particles start bumping because they cannot pass between the posts of the same row due to the action of the nDEP force (compare Figures 3 and 6b).

The particle behaviour changed completely at low frequencies (below 500 Hz), where their behaviour switched from zig-zag mode to displacement mode. We postulate that the EP/EO low frequency oscillation caused by the time varying orthogonal field leads to an increase in the effective diameter of the particles. For high enough voltages particles started to bump on the posts so that their trajectories deviate from the normal zig-zag mode. This effect is illustrated diagrammatically in Figure 3c which shows how the oscillations follow the field lines. This corresponds to the observations of particle trajectories seen in Figure 6c, where it is possible to appreciate the amplitude of the oscillation while the particles bump on the posts (compare with Figure 6b).

View Article Online
DOI: 10.1039/C8LC01416G

Separation of 3.0 µm, 1.0 µm and 500 nm particles

In order to characterise the system, the electrokinetically induced deviation angle for 1.0 µm and 3.0 µm diameter microspheres was measured as a function of applied frequency for different electrolyte conductivities. This was performed for a device of 6.3 µm critical diameter where all particles are expected to move in zig-zag mode. The deviation angle was measured by comparing the lateral position where the particles enter the channel to the position at the exit. This data is summarised in Figure 7.

Figures 7a and 7b show the deviation angles for 3.0 µm microspheres for electrolyte conductivities of 1.7 mS/m, 6.6 mS/m and 15.7 mS/m, for frequencies from 50 Hz to 500 kHz. For these conductivities, the 3.0 µm beads are always less polarisable than the surrounding medium at all frequencies, and therefore experience nDEP ($Re[\tilde{f}_{CM}] < 0$), as shown by the calculations in Figure 2. Figure 7a shows the deviation angle when the voltage applied to the electrodes was 320 Vpp. In this case, the deviation was always maximum for the entire range of frequencies for the three conductivities studied, i.e. the nDEP force was always strong enough to make the particles bump on the posts. The deviation at low frequencies was also maximum and no differences in the deviation angle were measured with respect to nDEP-induced deviation. Figure 7b shows data when the voltage was reduced to 120 Vpp. In this case the low frequency oscillation mechanism induced a displacement mode; the nDEP force was too weak and could not overcome the fluid drag force to prevent particles from zigzagging. Comparison of Figures 7a and 7b clearly indicates that the EP/EO oscillation-induced behaviour is independent of the nDEP-induced deviation. According to the current understanding of the polarisation of dielectric colloids, the dependence of the magnitude of the DEP force with field frequency is given by the Clausius-Mossotti factor, which in this case is assumed to be constant for the range of frequencies and the three conductivities studied in Figures 7a and 7b, down to low frequencies. A constant nDEP force cannot produce the data shown in Figure 7b; the low frequency oscillation induced by EP and EO causes the observed deviation found at low frequencies (in the range 50 Hz to 500 Hz). These electrophoretic and electroosmotic forces scale linearly with the magnitude of the electric field. However, the nDEP decreases much more rapidly (with E^2) and as a result the nDEP induced deviation becomes significant at higher voltages.

Figure 7c shows summary data for the induced deviation angle of smaller 1.0 µm beads in a 6.3 µm critical diameter DLD device as a function of frequency. The particles were suspended in an electrolyte with conductivities of 1.7 mS/m, 6.6 mS/m, 15.7 mS/m and 58 mS/m, and an applied voltage of 320 Vpp. This plot shows differences in the trajectories of particles that experience pDEP and nDEP. For 1.7 mS/m, $Re[\tilde{f}_{CM}] > 0$, deviation was only observed at low frequencies, caused by the EP/EO-induced oscillation. For higher frequencies, this oscillation became negligible and deviation ceases. For the 6.6 mS/m conductivity electrolyte $Re[\tilde{f}_{CM}]$ was only slightly negative and very close to 0 so the DEP force was insignificant, therefore only the very low frequency field induced a displacement mode. At higher medium conductivities, (15.7 mS/m and 58 mS/m), nDEP was significant and strong enough to make the particles switch from zig-zag to bumping mode.

View Article Online
DOI: 10.1039/C8LC01416G

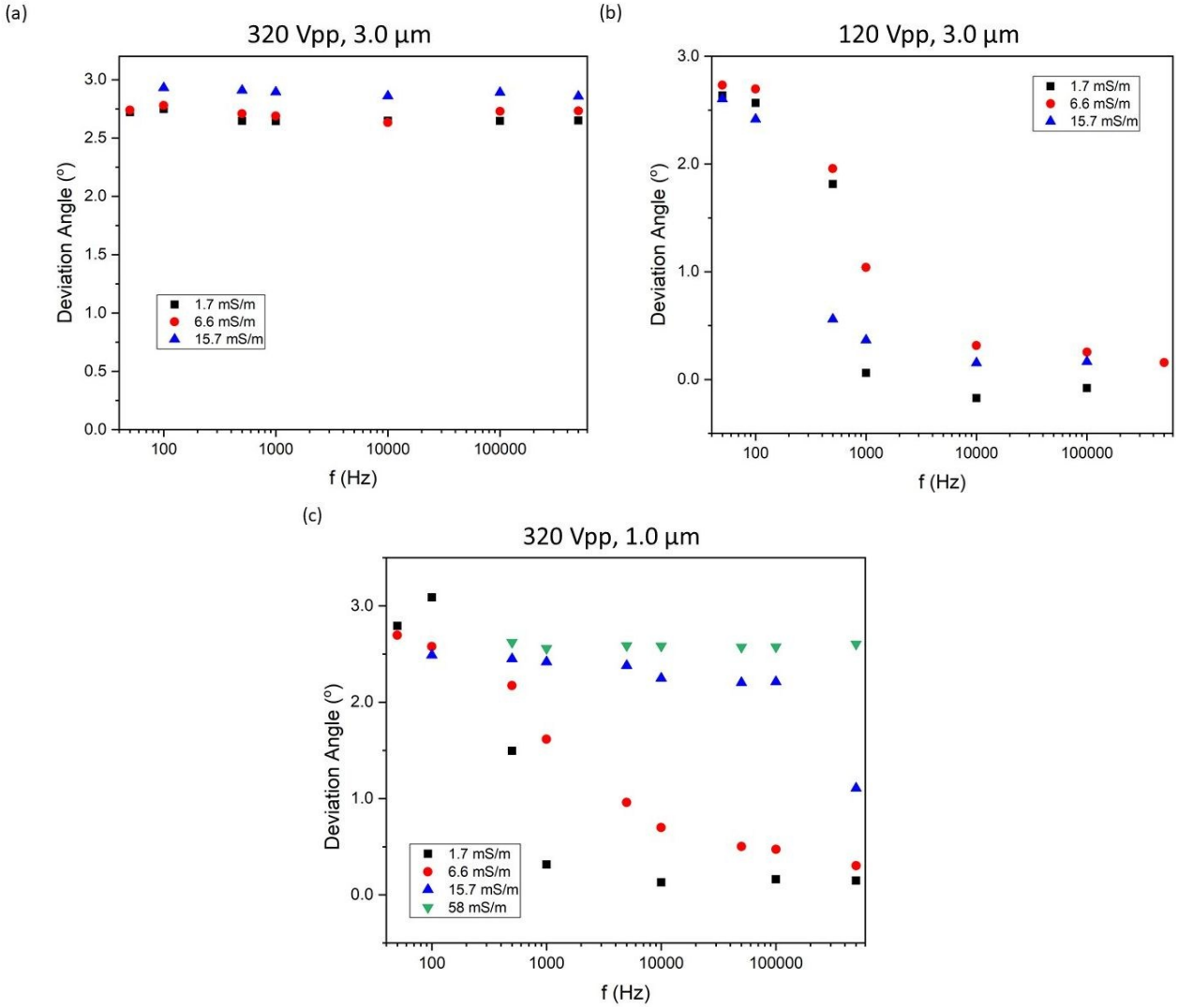

Figure 7 Electrokinetically induced deviation angle of 3.0 µm and1.0 µm diameter microspheres in a $D_c = 6.3\ \mu m$ DLD for different medium conductivities as a function of the frequency of the AC electric field. (a) 3.0 µm and 320 Vpp. (b) 3.0 µm and 120 Vpp. (c) 1.0 µm and 320 Vpp.

Figure 8 shows two examples of how this technique can be used to tune the separation of a classic DLD system. A mixture of 3.0 µm, 1.0 µm and 500 nm diameter microspheres suspended in an electrolyte of 1.7 mS/m conductivity were introduced in a 6.3 µm D_c DLD. The sequence of images in Figure 8a, 8b and 8c are separated by a distance of 5 mm apart along the device in the downstream direction, demonstrating the separation. Since the particles were smaller than the critical diameter, no deviation was observed in the absence of an electric field (Figure 8a). At the electrolyte conductivity of 1.7 mS/m only the 3.0 µm microspheres experience nDEP so when a signal of 320 Vpp and 10 kHz was applied, only these particles changed behaviour from zig-zag to bumping mode, leading to clear separation from the other particles (Figure 8b). When the frequency of the applied signal was reduced down to 50 Hz (with the same voltage of 320 Vpp), the 1.0 µm particles also switched to bumping mode due to the low frequency induced oscillation. At this voltage, the EP/EO force was not strong enough to induce significant deviation of the 500 nm microspheres that continued to flow in zig-zag mode. Figure 8c shows this mode of operation where both the 1.0 µm and 3.0 µm particles are separated from the 500nm particles. These results match perfectly with the deflection angle data shown in Figure 7, and comparison of Figures 8a, 8b and 8c clearly demonstrate the potential of the technique for continuous flow particle separation. The results show that the separation of micron-sized particles in DLD channels with a critical diameter larger than the particle size can be controlled using AC electric induced forces generated orthogonal to the fluid flow. In this way, the effective critical diameter of the device D_c can be controlled by changing the magnitude or frequency of the electric field turning the DLD device into a tunable device and where differences in both the size and electrokinetic properties of particles can be exploited for sorting.

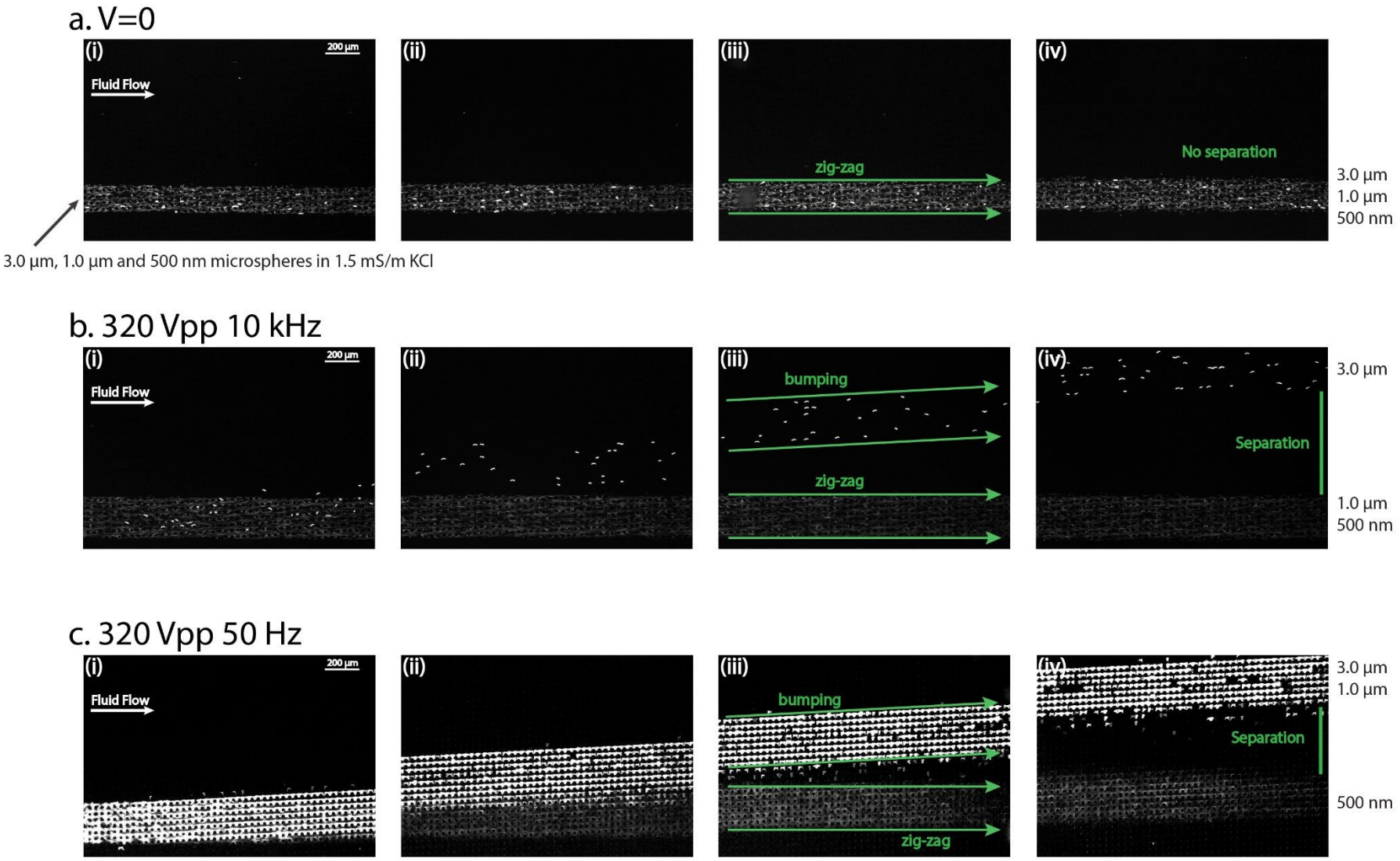

Figure 8. AC electrokinetic induced deviation of 3.0 µm, 1.0 µm and 500 nm microspheres suspended in 1.7 mS/m electrolyte conductivity in a 6.3 µm critical diameter DLD. Each set of images in the three series was taken by scanning along the device in the downstream in 5 mm steps. (a) No electric field applied – All the particles flow parallel to the fluid flow since they are smaller than the critical diameter of the device. (b) 320 Vpp and 10 kHz applied signal – particles of 3.0 µm are separated from the mixture of 1.0 µm and 500 nm spheres due to nDEP. (c) 320 Vpp and 50 Hz applied signal – particles of 3.0 µm and 1.0 µm are separated from the 500 nm microspheres due to the low frequency oscillation.

View Article Online
DOI: 10.1039/C8LC01416G

Conclusions and outlook

We have demonstrated a Deterministic Lateral Displacement device with integrated electrodes to generate electrokinetic forces that can deflect particles based on a combination of Electrophoresis, Electroosmosis and Dielectrophoresis. The technique was characterised for two different particle sizes (3.0 μm and 1.0 μm, both smaller than the critical diameter D_c) and different electrolyte conductivities. Selective separation of 3.0 μm and 1.0 μm and 500 nm microspheres was also demonstrated. For high frequency AC electric fields and sufficiently high electrolyte conductivity, all the particles experience nDEP. Varying the applied voltage modifies the effective critical diameter of the DLD leading to a tunable separation system. With low electrolyte conductivities, particles can be separated depending on their electrical polarizability. If particles experience either weak nDEP or pDEP they do not deviate and follow the fluid flow in zig-zag mode. Particles that experience a significant nDEP force change behaviour and bump along the posts. In this respect, particle behaviour is similar to iDEP, except that the DLD device provides a means for high throughput continuous-flow separation.

Interestingly at low frequencies (< 500 Hz) the EP/EO induced particle oscillation leads to significant perturbation of the particle trajectories. Preliminary results indicate that the deviation depends strongly on the oscillation amplitude, which increases the effective particle diameter. This EP/EO behaviour suggests that differences in particle zeta potential could also be exploited for particle separation. The method shows promise for rapid and high throughput separation of micron- or even nano-sized particles in continuous flow. Future work will include a full theoretical and numerical analysis of the forces involved in the separation mechanism, with the aim of quantitatively describing the oscillation-induced deviation. A fuller understanding of the physics that underlies the combination of DLD and electrokinetics will lead to new device designs that will extend the range of potential applications.

Authors contribution

V.C. and H.M. designed the DLD devices and planned the experiments. V.C. performed the experiments and analysed the data. C.H. helped with the design of the DLD devices, designed the electrodes and provided experimental support. P.G. and A.R. were involved in planning and supervised the work. V.C., P.G., A.R. and H.M., interpreted the experimental results, conceptualized the ideas, developed the theoretical framework and wrote the manuscript.

Conflict of interest

The authors declare no conflict of interest.

Acknowledgments

We acknowledge Bao Dang Ho, Jason P. Beech and Jonas O. Tegenfeldt from University of Lund for valuable discussion. P.G.S. and A.R. acknowledge financial support from Spanish Government Ministry MEC under Contract FIS2014-54539P.

References

1 L. R. Huang, E. C. Cox, R. H. Austin and J. C. Sturm, *Science (80-.).*, 2004, **304**, 987–990.

2 D. W. Inglis, J. A. Davis, R. H. Austin and J. C. Sturm, *Lab Chip*, 2006, **6**, 655–658.

3 D. W. Inglis, *Appl. Phys. Lett.*, 2009, **94**, 013510.

4 J. McGrath, M. Jimenez and H. Bridle, *Lab Chip*, 2014, **14**, 4139–4158.

5 K. Loutherback, K. S. Chou, J. Newman, J. Puchalla, R. H. Austin and J. C. Sturm, *Microfluid. Nanofluidics*, 2010, **9**, 1143–1149.

6 Z. Liu, F. Huang, J. Du, W. Shu, H. Feng, X. Xu and Y. Chen, *Biomicrofluidics*, 2013, **7**, 11801.

7 K. K. Zeming, S. Ranjan and Y. Zhang, *Nat. Commun.*, 2013, **4**, 1625–1628.

8 K. K. Zeming, T. Salafi, C. H. Chen and Y. Zhang, *Sci. Rep.*, 2016, **6**, 1–10.

View Article Online
DOI: 10.1039/C8LC01416G

9 K. K. Zeming, N. V. Thakor, Y. Zhang and C. H. Chen, *Lab Chip*, 2016, **16**, 75–85.
10 D. Holmes, G. Whyte, J. Bailey, N. Vergara-Irigaray, A. Ekpenyong, J. Guck and T. Duke, *Interface Focus*.
11 B. H. Wunsch, J. T. Smith, S. M. Gifford, C. Wang, M. Brink, R. L. Bruce, R. H. Austin, G. Stolovitzky and Y. Astier, *Nat. Nanotechnol.*, 2016, **11**, 936–940.
12 R. Devendra and G. Drazer, *Anal. Chem.*, 2012, **84**, 10621–10627.
13 J. P. Beech and J. O. Tegenfeldt, *Lab Chip*, 2008, **8**, 657–659.
14 J. P. Beech, P. Jönsson and J. O. Tegenfeldt, *Lab Chip*, 2009, **9**, 2698–2706.
15 B. H. Lapizco-Encinas, *Electrophoresis*, 2018, 1–18.
16 R. P. and Y. H. and X. W. and J. P. H. Burt, *J. Phys. D. Appl. Phys.*, 1992, **25**, 881.
17 B. A. Simmons, G. J. McGraw, R. V Davalos, G. J. Fiechtner, Y. Fintschenko and E. B. Cummings, *MRS Bull.*, 2006, **31**, 120–124.
18 S. Masuda, M. Washizu and T. Nanba, *IEEE Trans. Ind. Appl.*, 1989, **25**, 732–737.
19 E. B. Cummings and A. K. Singh, 2000, vol. 4177, pp. 4110–4177.
20 E. B. Cummings and A. K. Singh, *Anal. Chem.*, 2003, **75**, 4724–4731.
21 E. B. Cummings, *IEEE Eng. Med. Biol. Mag.*, 2003, **22**, 75–84.
22 B. H. Lapizco-Encinas, R. V. Davalos, B. A. Simmons, E. B. Cummings and Y. Fintschenko, *J. Microbiol. Methods*, 2005, **62**, 317–326.
23 B. H. Lapizco-Encinas, B. A. Simmons, E. B. Cummings and Y. Fintschenko, *Anal. Chem.*, 2004, **76**, 1571–1579.
24 B. H. Lapizco-Encinas, S. Ozuna-Chacón and M. Rito-Palomares, *J. Chromatogr. A*, 2008, **1206**, 45–51.
25 S. K. Srivastava, J. L. Baylon-Cardiel, B. H. Lapizco-Encinas and A. R. Minerick, *J. Chromatogr. A*, 2011, **1218**, 1780–1789.
26 N. Lewpiriyawong, C. Yang and Y. Lam Cheong, *Biomicrofluidics*, , DOI:10.1063/1.2973661.
27 B. G. Hawkins, A. E. Smith, Y. A. Syed and B. J. Kirby, *Anal. Chem.*, 2007, **79**, 7291–7300.
28 L. M. Barrett, A. J. Skulan, A. K. Singh, E. B. Cummings and G. J. Fiechtner, *Anal. Chem.*, 2005, **77**, 6798–6804.
29 C. Church, J. Zhu, G. Wang, T. R. J. Tzeng and X. Xuan, *Biomicrofluidics*, , DOI:10.1063/1.3267098.
30 J. Zhu and X. Xuan, *Biomicrofluidics*, 2011, **5**, 24111.
31 S. Kim, B. H. Wunsch, H. Hu, J. T. Smith, R. H. Austin and G. Stolovitzky, *Proc. Natl. Acad. Sci.*, 2017, **114**, E5034–E5041.
32 J. A. Davis, PhD thesis, Princeton University, 2008.
33 R. J. Hunter, *Foundations of colloid science*, Oxford university press, 2001.
34 H. Morgan and N. G. Green, *AC electrokinetics*, Research Studies Press, 2003.
35 I. Ermolina and H. Morgan, *J. Colloid Interface Sci.*, 2005, **285**, 419–428.
36 R. W. O'Brien and L. R. White, *J. Chem. Soc. Faraday Trans. 2 Mol. Chem. Phys.*, 1978, **74**, 1607–1626.
37 R. Pethig, *Biomicrofluidics*, 2010, **4**, 22811.
38 J. J. Lyklema, *Fundamentals of Interface and Colloid Science Vol. II: Solid–Liquid Interface*, Academic Press, 1995, vol. II.
39 C. T. O'Konski, *J. Phys. Chem.*, 1960, **64**, 605–619.
40 H. Zhao, *Electrophoresis*, 2011, **32**, 2232–2244.
41 V. N. Shilov, A. V. Delgado, F. González-Caballero, J. Horno, J. J. López-García and C. Grosse, *J. Colloid Interface Sci.*, 2000, **232**, 141–148.